Journal of Power Sources 232 (2013) 99–105

Contents lists available at SciVerse ScienceDirect

Journal of Power Sources

journal homepage: www.elsevier.com/locate/jpowsour

Highly active PdAu alloy catalysts for ethanol electro-oxidation

Yuan-Yuan Feng*, Zeng-Hua Liu, Yang Xu, Ping Wang, Wen-Hui Wang, De-Sheng Kong

Key Laboratory of Life-organic Analysis, College of Chemistry and Chemical Engineering, Qufu Normal University, Qufu, Shandong 273165, China

HIGHLIGHTS

- Alloyed Pd_mAu NPs are prepared through the co-reduction of K_2PdCl_4 and $HAuCl_4$ precursors.
- The addition of Au into Pd catalysts improves the catalytic activity and stability of Pd for EOR.
- Proper proximity and relative amount of Au and Pd are crucial for the promotion effect of Au.

ARTICLE INFO

Article history:
Received 22 July 2012
Received in revised form
11 December 2012
Accepted 2 January 2013
Available online 10 January 2013

Keywords:
Electrocatalyst
Alloy
Palladium
Gold
Ethanol electro-oxidation reaction

ABSTRACT

Alloyed Pd_mAu nanoparticles (m refers to the atomic Pd/Au ratio), prepared through the co-reduction of K_2PdCl_4 and $HAuCl_4$ precursors in aqueous solutions, are employed as the catalysts for ethanol electro-oxidation reaction (EOR) in alkaline electrolyte. Transmission electron microscopy (TEM) and X-ray diffraction (XRD) are used to characterize the morphology and confirm the alloy structure of the samples. Cyclic voltammetry (CV) and chronoamperometry (CA) results indicate that the addition of Au to Pd can significantly improve the catalytic activity of Pd toward EOR and the improvement is strongly dependent on the composition of the catalysts. $Pd_{1.0}Au/C$ is identified as the most efficient catalyst since it produces the highest catalytic activity and long-term stability. The mass-specific activity (MSA) and intrinsic activity (IA) data of $Pd_{1.0}Au/C$ is 1.45 mA μg^{-1}_{Pd+Au} and 80.2 A m^{-2}_{Pd}, which is found to be 2.3 and 11.3 times that of the Pd/C catalyst, respectively. These findings clearly suggest that the proximity and relative amount of Au and Pd on the surface of the nanoparticles (NPs) are crucial for the improvement of Pd catalysis, which would have important implications for designed preparation of bimetallic catalysts for the direct alcohol fuel cells.

1. Introduction

Direct alcohol fuel cells (DAFCs) with the electro-oxidation of small liquid organic molecules as the anode reaction have attracted much attention in recent years due to the much higher energy density of liquid fuels than gaseous fuels such as hydrogen [1]. Among the anodic organic molecules, ethanol as a kind of major renewable biofuel is thought to be very promising for the development of fuel cells because it is less toxic than methanol and can be produced from the fermentation of biomass [2]. To date, Pt is the most widely used catalyst material for the electro-oxidation of methanol and ethanol [3–5]. However, the high cost and low durability of Pt hinder the large-scale manufacturing and development of the DAFCs. In recent years, many investigations have focused on the development of non-platinum electrocatalysts for anodic and cathodic reactions of fuel cells [6–8]. Among the non-platinum materials, Pd is the most Pt-like metal and a relatively abundant resource. Although Pd catalysts appear less active toward the cathodic oxygen reduction reaction (ORR), it possesses superior catalytic activity toward the anodic alcohol electro-oxidation especially in alkaline electrolyte [9–11]. Since the price of Pd is currently about one-third that of Pt, it is worth to develop such non-platinum material as electrocatalysts for DAFCs.

Optimizing the nanostructures has been a major issue in improving the catalytic performance of the electrocatalysts. Introducing a second metal into Pd to form bimetallic nanomaterials has become a widely accepted method to prepare the highly active Pd-based electrocatalysts, such as Pd-based core–shell nanostructures or Pd-based alloy [12–16]. Zhao et al. have proved that the addition of Ir to Pd can significantly improve the ethanol oxidation kinetics on Pd in alkaline electrolyte [15], the promoted effect mainly arises from the bifunctional mechanism while the electronic effect contributes little to the highly catalytic activity of the PdIr/C catalysts. It is widely accepted that for the bimetallic catalysts, two kinds of

* Corresponding author. Tel./fax: +86 537 4458301.
E-mail address: yfeng@mail.tsinghua.edu.cn (Y.-Y. Feng).

0378-7753/$ – see front matter © 2013 Elsevier B.V. All rights reserved.
http://dx.doi.org/10.1016/j.jpowsour.2013.01.013

effects, *i.e.* ligand and geometric effects, are considered as the root causes of the enhancement in the activity and stability of the catalysts [17,18]. The ligand effects, induced by electronic charge transfer between the individual components of an alloy, could lead to rational modification of the electronic structure of the catalysts [19–21]. The geometric effects including the particle morphology (particle size or dispersion state), interatomic distance, coordination environment and lattice strain are also important. Due to the electronic and geometric effects induced by the promoter, the catalytic activity and stability of the catalysts can be significantly improved.

In this work, a series of bimetallic Pd_mAu alloy catalysts (m refers to the atomic Pd/Au ratio, $m = 0.1$–1.5) are prepared by reductive of K_2PdCl_4 and $HAuCl_4$ in aqueous solution and screened for ethanol electro-oxidation reaction (EOR) in alkaline electrolyte. We disclose that the bimetallic Pd_mAu catalysts exhibit much higher catalytic activity and stability than monometallic Pd catalyst for EOR and the proximity of the Pd and Au atoms is of vital importance to the promotion effect of Au.

2. Experimental

For the preparation of Pd_mAu alloy samples, 0.5 mL K_2PdCl_4 (0.01 M), 1.0 mL $HAuCl_4$ (0.05 M) and 9.2 mL PVP (0.6 M) were mixed and diluted to 100 mL with deionized water. After stirring for 30 min, 5 mL $NaBH_4$ solution (0.1 M) was added dropwise under vigorous stirring to synthesize the $Pd_{0.1}Au$ colloids. Carbon-supported $Pd_{0.1}Au$ sample ($Pd_{0.1}Au/C$) was prepared by mixing the as-formed $Pd_{0.1}Au$ colloids with a desired amount of Vulcan XC-72 carbon. Then, the suspension was refluxed for 4 h. The powders were separated by filtration, followed by intensive washing with deionized water and air-drying at 110 °C for 2 h. For the whole series of samples, Au loading was kept at approximately 20 wt. %, while the molar ratio of Pd precursor was changed. The reference Pd/C (10 wt. % of Pd) and Au/C samples were prepared through the same method only the Au or Pd precursors were not added into the solution.

The morphology of the Pd_mAu/C nanostructures was investigated using JEM-2100 transmission electron microscope (TEM) operating at 120 kV. X-ray diffraction (XRD) patterns were measured with a D8-Advance Bruker diffractometer at a scan rate of 4 deg min^{-1} ($30° < 2\theta < 85°$) and the wavelength of the incident radiation was 1.5406 Å (Cu Kα). The actual loading amount and composition of Pd and Au in the as-prepared carbon supported catalysts were determined by inductively coupled plasma atomic emission spectrometry (ICP-AES, Perkin Elmer Optima-4300DV Spectrometer). X-ray photoelectron spectroscopy (XPS) measurements were carried out on Thermo ESCALAB 250 instrument equipped with Al Kα radiation ($h\nu = 1486.6$ eV).

Glassy carbon (GC) electrode ($d = 5$ mm) was polished with 0.5 and 0.05 μm alumina suspensions prior to each use, followed by washing ultrasonically with HNO_3 (1:1), ethanol, acetone and deionized water, sequentially. The catalyst ink was prepared by sonicating a suspension of the carbon-supported catalyst (5.0 mg) in isopropanol (1.0 mL). 10 μL of the suspension was firstly transferred onto the disk electrode, after the solvent evaporation at room temperature, 10 μL 0.05 wt. % Nafion solution (Dupont) was then pipetted onto the catalyst layer and air-dried.

Electrochemical measurements including cyclic voltammetry (CV) and chronoamperometry (CA) were carried out in a conventional three-electrode cell using CHI 660A at room temperature. A Pt foil (1.0 cm × 1.0 cm) and a saturated calomel electrode (SCE) were used as the counter electrode and reference electrode, respectively. All potentials mentioned in this work are given with respect to the SCE. The electrolyte was 0.5 M KOH + 2.0 M CH_3CH_2OH solution. The CV curves were recorded in the potential between −1.0 and 0.6 V (scan rate: 20 mV s^{-1}), and the CA analyses were carried out at −0.5 V vs. SCE.

3. Results and discussion

3.1. Morphology and structural characterizations of the Pd_mAu/C samples

Fig. 1 shows the morphologic features of two representative Pd_mAu/C samples ($m = 0.1$ and 1.0). The corresponding metal nanoparticle (NP) size distributions are shown in the bar-graph on the right. The metal particles exhibited a spherical-like shape and were dispersed on the support without significant aggregation. The mean metal particle sizes were evaluated from an ensemble of at least 200 particles in an arbitrarily chosen area of the corresponding TEM images. For the $Pd_{0.1}Au/C$ and $Pd_{1.0}Au/C$ samples, the mean metal particle size was 9.2 ± 1.6 nm and 9.5 ± 1.5 nm, respectively. For the other Pd_mAu/C samples, the mean particle sizes were slightly different (9.2–9.5 nm) whereas the shapes of the size distributions were almost the same, showing a good monodispersity of the particles.

Fig. 2A presents the XRD patterns of Pd_mAu/C, Pd/C and Au/C samples in the range of $30° < 2\theta < 85°$. Each XRD pattern exhibited four diffraction peaks which could be indexed to diffraction from the (111), (200), (220) and (311) of the face-centered cubic (fcc) structure of metallic Au and/or Pd. As m increases, the diffraction peaks of the Pd_mAu particles exhibited a shift from pure Au ($2\theta = 38.1$, 44.2, 64.4 and 77.5) to pure Pd ($2\theta = 39.8$, 46.2, 67.8 and 81.8), indicative of the formation of an alloy structure. The magnified (111) peaks of the samples are shown in Fig. 2B. These phenomena were similar to the XRD results of Au–Pd alloy reported by Zhang et al. [22] and Lee et al. [23]. In addition, most diffraction peaks of the alloys were symmetric while some peaks appeared asymmetric or broadened especially for the $Pd_{1.0}Au/C$ sample, which may be due to the structural defects on the surface of the NPs or the small crystallite sizes. The average crystallite sizes can be calculated from the (111) facet diffraction peaks using Scherrer's equation:

$$d = \frac{0.9\lambda_{k\alpha 1}}{B_{2\theta}\cos\theta_{\max}}$$

where λ is the wavelength of the X-ray (1.54056 Å), $B_{2\theta}$ is the width of the peak at half-height, and θ is the angle at the maximum of the peak. The crystallite sizes of the Pd_mAu/C samples with a relatively high m ($m \geq 0.5$) were 8.0–8.6 nm, which were slightly smaller than that of $Pd_{0.1}Au/C$ (9.0 nm), and also slightly smaller than the corresponding particle sizes obtained from the TEM images. For the Pd_mAu/C with low m ($m = 0.1$), the crystallite size (9.0 nm) was in good agreement with the particle size obtained from the TEM images (9.2 nm).

3.2. Electrochemical characterizations

Fig. 3 shows the cyclic voltammograms of the Pd_mAu/C samples in 0.5 M KOH solution free of ethanol. The peaks appearing in the low potential side featured the hydrogen absorption and adsorption on Pd in the catalysts since the Au surface is inactive for hydrogen adsorption/absorption. The shapes of this hydrogen region were similar to those reported in previous publication [24]. For the Pd_mAu/C catalysts with a relatively low m ($m \leq 0.5$), the hydrogen region was not pronounced while for the Pd_mAu/C catalysts with high m ($m \geq 1.0$), the profile of the hydrogen adsorption/absorption was well-defined. The most negative anodic peak

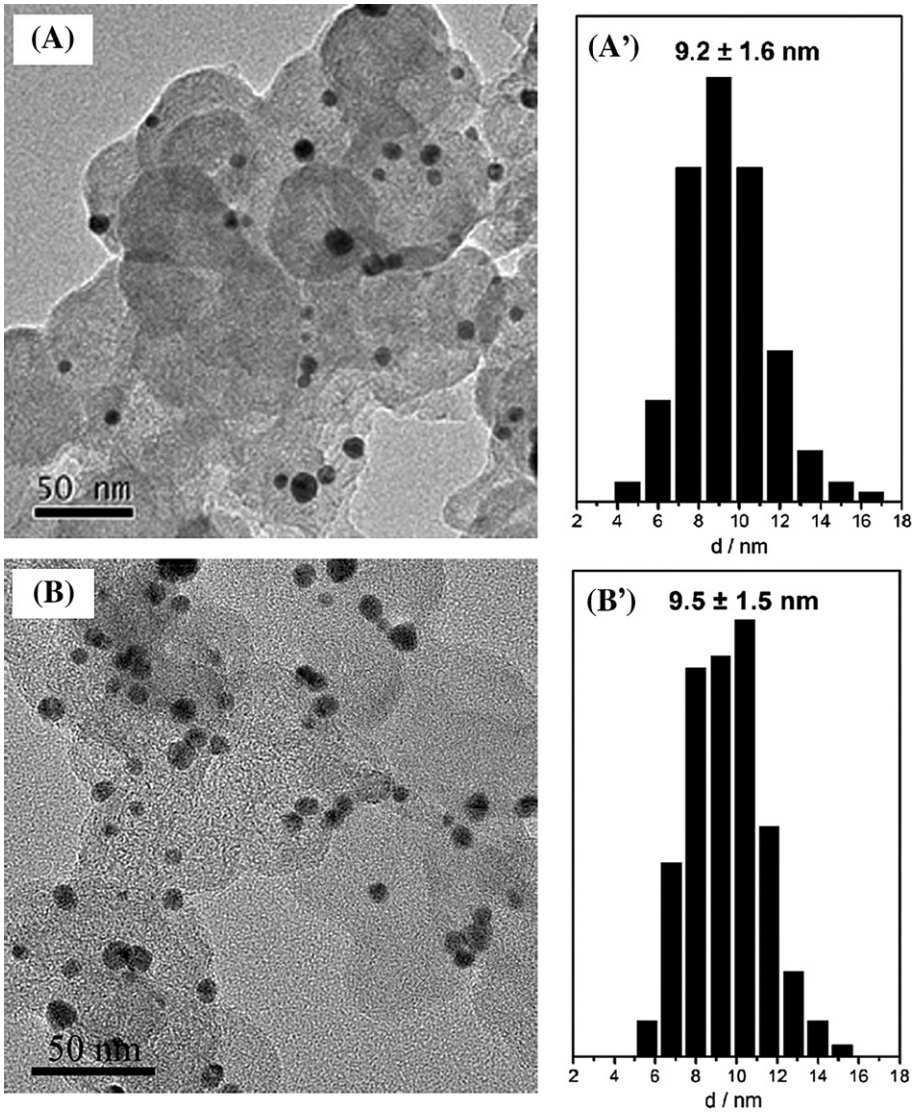

Fig. 1. Representative TEM images of $Pd_{0.1}Au/C$ (A) and $Pd_{1.0}Au/C$ (B) samples. The corresponding size histograms for the metal particles are shown in the bar-graph on the right.

originated from the oxidation of absorbed hydrogen and the two anodic peaks at relatively high potentials were related to the oxidation of adsorbed hydrogen on the surface of Pd [24–26]. Since the peak position of hydrogen adsorption is very close to that of hydrogen absorption, it is difficult to separate their contributions simply through the integration method, which is usually used to measure the electrochemically active surface area (EAS) of Pt. In the hydrogen region, besides the anodic peaks of hydrogen absorption and adsorption, two pronounced cathodic peaks were also detected. The cathodic peak at −0.77 V should arise from the hydrogen adsorption and another cathodic peak at more negative potential corresponded to the hydrogen absorption and evolution.

In the relatively high potential range of the voltammograms, two kinds of cathodic peaks appeared. The broad cathodic peaks at *ca*. 0.15 V were associated with the reduction of Au oxides [27], the strong cathodic peaks appearing from −0.32 to −0.07 V originated from the reduction of Pd oxides [28]. Due to the different Pd dispersion state on the surface of the catalysts, the positions of these cathodic peaks corresponding to the reduction of Pd oxides were somewhat different. And with increasing *m*, this peak shifted to the negative potential slightly. Since the electric quantity of this cathodic peak corresponds to the amount of charge needed to reduce the Pd oxides formed on the NP surface during the positive-going potential scan, the surface area of Pd in the catalysts can be calculated by dividing the amount of reduction charge (Q_r) by its conversion factor of *ca*. 4.24 C m^{-2} [29]. The EAS of Pd can then be measured according the following equation:

$$\mathrm{EAS}\left(\mathrm{m^2\ g_{Pd}^{-1}}\right) = Q_r / \left(4.24\ \mathrm{C\ m^{-2}} \times W_{\mathrm{Pd}}\right)$$

where W_{Pd} is the Pd loading by mass (weight in grams) at the working electrode. With increasing *m*, the EAS of Pd increased from 67 $m^2\ g^{-1}{}_{Pd}$ at $m = 0.1$ to 81 $m^2\ g^{-1}{}_{Pd}$ at $m = 0.5$, and then to 132 $m^2\ g^{-1}{}_{Pd}$ at $m = 1.0$, suggesting a gradual increase in the fraction of exposed Pd atoms on the NP surfaces. However, when *m* further increased to 1.5, the EAS of Pd did not continue to increase but decreased to 99 $m^2\ g^{-1}{}_{Pd}$. Since only the exposed Pd atoms at the surface could be accessible for the electrochemical reactions and contribute to the surface area of Pd, the surface atomic Pd/Au ratio (surface composition) became a key to understanding this interesting EAS order of Pd_mAu/C sample. XPS,

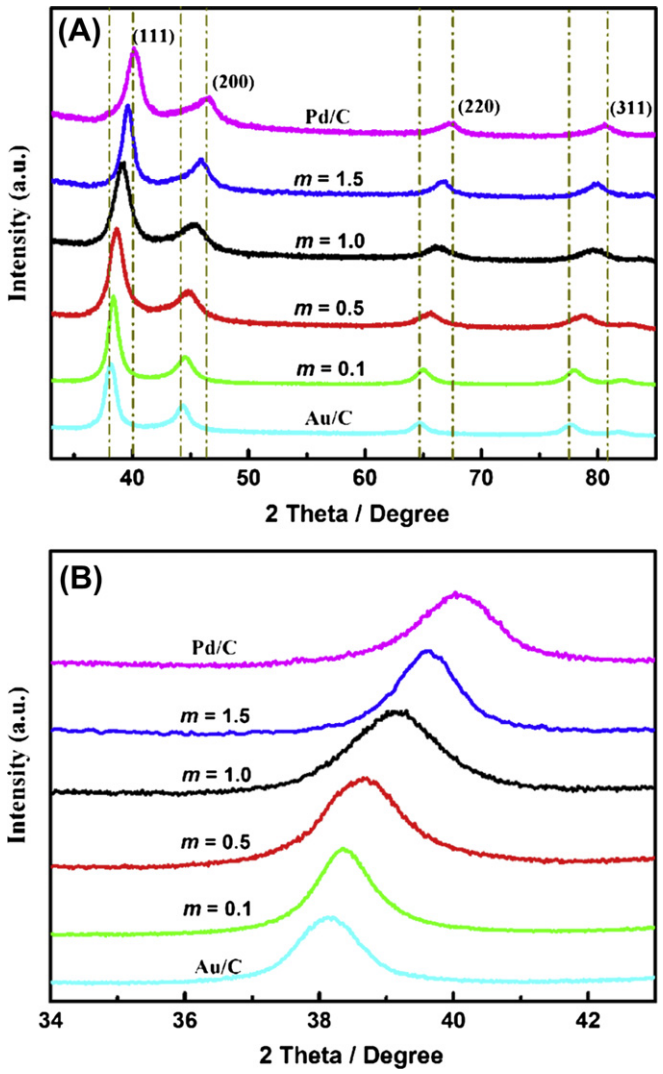

Fig. 2. XRD patterns (A) and the magnified (111) peaks (B) of the Pd_mAu/C, Au/C and Pd/C samples.

as a powerful surface analysis technique, could give the surface composition of the samples (Fig. 4). The surface atomic Pd/Au ratios detected from XPS are 0.57, 1.86 and 2.71 for the samples with $m = 0.5$, 1.0 and 1.5, respectively (The content of Pd in $Pd_{0.1}Au/C$ sample was too low to be detected and thus not shown here), suggesting that the surfaces of the Pd_mAu/C samples are enriched with Pd, as compared with their bulk compositions. Two inverse effects could be responsible for the differences between the surface and bulk composition. The preparation procedure would be the main factor that leads to the Pd-enriched surfaces. The reduction potential of $AuCl_4^-/Au$ is 1.00 V vs. SHE (standard hydrogen electrode), which is much higher than that of $PdCl_4^{2-}/Pd$ (0.59 V vs. SHE), the formation of the alloy NPs might be initiated by Au-enriched inner and then Pd-enriched surface. Similar results were also found by Lee and co-workers [23]. However, an inverse effect arising from the differences in the surface free energy of Au and Pd could not be neglected. The surface free energy of Au (1.626 J m^{-2}) is lower than that of Pd (2.043 J m^{-2}) [30–32], the Au atoms preferentially segregate to the surface of the NPs to minimize the surface free energy especially during the process of refluxing. It is reported that for the Pd_mAu/C samples with relatively low content of Au (high m), the degree of Au segregation to the surface was higher than those with high content of Au (low m) [33], which would lead to the decrease in the proportion of the exposed Pd atoms at the surface of the Pd_mAu/C with relatively high m (e.g. $Pd_{1.5}Au/C$), as compared with that in the Pd_mAu/C with low m (e.g. $Pd_{1.0}Au/C$). Thus, the EAS of Pd in $Pd_{1.5}Au/C$ would be lower than that in $Pd_{1.0}Au/C$.

The cyclic voltammograms of the Pd_mAu/C catalysts for EOR in 0.5 M KOH with 2 M CH_3CH_2OH electrolyte are shown in Fig. 5A. The data of the monometallic Pd/C and Au/C catalysts are also included for comparison. The peak potentials for EOR on the Pd_mAu/C and Pd/C catalysts were more negative than that observed on reference Au/C catalyst (0.26 V), suggesting that Pd in these catalysts are much more active than Au catalyst. For the $Pd_{0.1}Au/C$ catalyst, two separated anodic EOR peaks at −0.09 and 0.26 V should originate from the individual contribution of Pd and Au, respectively. Although the atomic Pd/Au ratio on the surface of $Pd_{0.1}Au/C$ NPs was *ca.* 0.57, the EOR currents originated from Pd and Au were almost the same. This further indicated that the catalytic activity of Pd was much higher than that of Au. For the other Pd_mAu/C catalysts with high m ($m = 0.5$, 1.0, 1.5), only one pronounced peak at *ca.* 0 V in the forward scan was given, and the

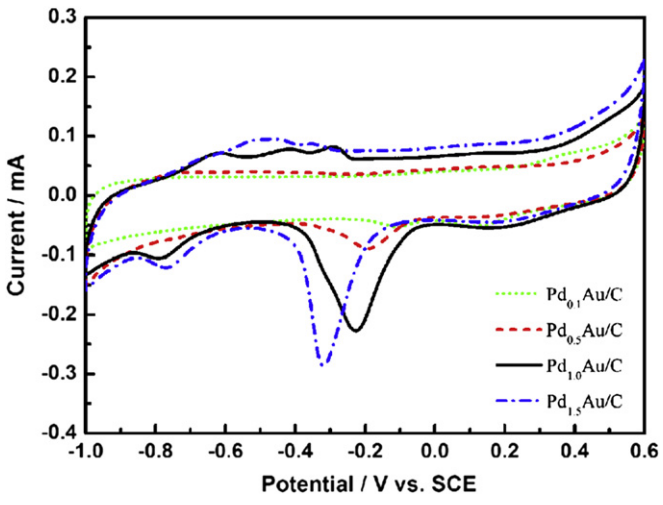

Fig. 3. Cyclic voltammograms of the Pd_mAu/C catalysts in 0.5 M KOH.

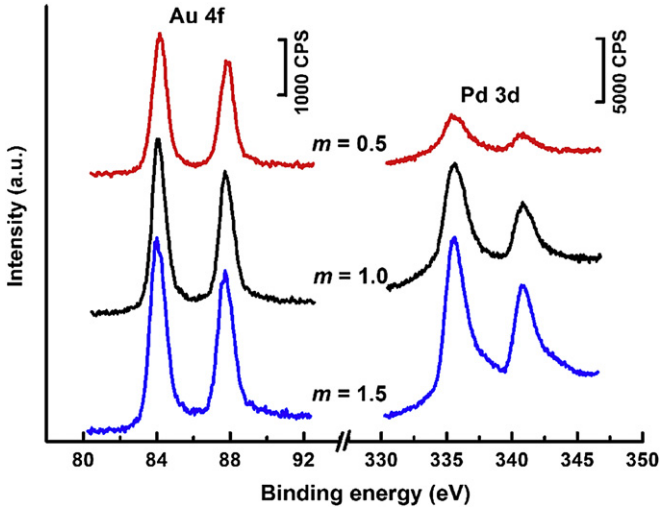

Fig. 4. Pd 3d and Au 4f XPS spectra for Pd_mAu/C samples.

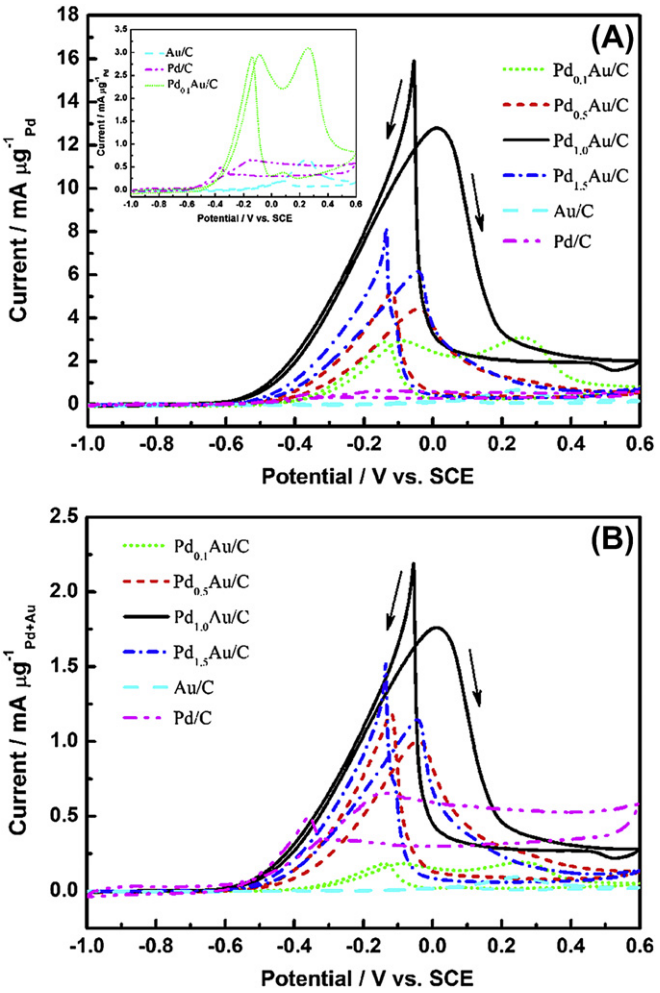

Fig. 5. Cyclic voltammograms of the Pd$_m$Au/C, Au/C and Pd/C catalysts in 0.5 M KOH + 2.0 M CH_3COOH with the currents normalized to the mass of Pd (A) and the total mass of Pd and Au (B) on the surface of the electrode. The inset in (A) shows the enlarged version for Au/C, Pd/C and Pd$_{0.1}$Au/C catalysts.

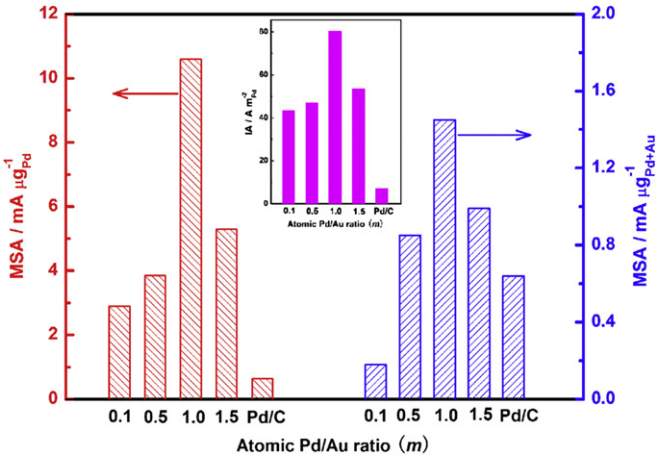

Fig. 6. Comparison of the mass-specific activities (MSAs) calculated at −0.1 V of the Pd$_m$Au/C and Pd/C catalysts. The inset shows the corresponding intrinsic activities (IAs) of the catalysts.

onset potentials were more negative than that on the monometallic Pd/C catalyst, indicating a much higher catalytic activity of Pd in these catalysts toward EOR. In addition, the peak shapes in the forward CV curves were not symmetrical as the currents dropped sharply after reaching the peak currents, especially for the Pd$_m$Au/C catalysts with a relatively high m. One possible reason for this phenomenon would be the decrease in ethanol concentration caused by the rapid consumption of ethanol on the catalysts [34]. For the backward scan of the CV curves, the anodic currents of all Pd$_m$Au/C catalysts showed a sharp increase, which may arise from the rapid removal of the adsorbed carbonaceous species not completely oxidized in the forward scan. This phenomenon was similar to that of the formic acid electro-oxidation on Pd-based catalysts [35–37] and implied that EOR on the Pd$_m$Au/C catalysts might not proceed a direct oxidation path to CO_2 [11,14].

Since the catalytic activity of the Pd$_m$Au/C catalysts mainly comes from the contribution of Pd, the EOR currents (−0.1 V) normalized to the mass of Pd on the working electrode were calculated and presented in the left half of Fig. 6. All of the Pd$_m$Au/C catalysts exhibited a much higher MSA than the monometallic Pd/C catalyst. The MSA data of the most active Pd$_{1.0}$Au/C catalyst (10.6 mA μg$^{-1}_{Pd}$) was about 16.6 times that on the monometallic Pd/C catalyst. For the other three Pd$_m$Au/C catalysts (m = 0.1, 0.5 and 1.5), the MSA is 2.9, 3.9 and 5.3 mA μg$^{-1}_{Pd}$, which is 4.5, 6.1 and 8.3 times that on the monometallic Pd/C catalyst, respectively. The above data indicated that the addition of Au could significantly improve the catalytic activity of Pd toward EOR. However, for the Pd$_m$Au/C catalysts, such comparisons seem not convincing since the promoter Au is also very expensive, which did not help to reduce the cost of the catalysts of fuel cells. Therefore, taking the total mass of Au and Pd in the Pd$_m$Au/C catalysts into account was reasonable and necessary.

Fig. 5B shows the cyclic voltammograms of the Pd$_m$Au/C catalysts for EOR with the currents were normalized to the total mass of Pd and Au on the working electrode. The relationship between the MSA data and m were presented in the right half of Fig. 6. Compared with the monometallic Pd/C catalyst, Pd$_{0.1}$Au/C showed a much lower catalytic activity whereas those Pd$_m$Au/C catalysts with relatively high m ($m \geq 0.5$) still appeared more active than the Pd/C catalyst. Pd$_{1.0}$Au/C catalyst showed the highest MSA (1.45 mA μg$^{-1}_{Pd+Au}$), which was *ca.* 2.3 times that of the Pd/C catalyst (0.64 mA μg^{-1}). The intrinsic activity (IA) of Pd, defined as the current normalized by the Pd EAS, are presented in the inset of Fig. 6. The IA data of Pd in the Pd$_m$Au/C catalysts were much higher than that of Pd/C, indicating that the Pd$_m$Au/C catalysts are intrinsically more active for EOR due to the presence of Au. The generally accepted electro-oxidation mechanism of ethanol in alkaline electrolyte can be summarized as follows [15,38,39]:

$$C_2H_5OH + 3OH^- \rightarrow CH_3CO_{ads} + 3H_2O + 3e^- \quad (1)$$

$$OH^- \rightarrow OH_{ads} + e^- \quad (2)$$

$$CH_3CO_{ads} + OH_{ads} \rightarrow CH_3COOH \quad (3)$$

$$CH_3COOH + OH^- \rightarrow CH_3COO^- + H_2O \quad (4)$$

The rate-determining step is Eq. (3). That is, the EOR is determined by the removal of the adsorbed intermediate species CH_3CO_{ads}, which is dependent on the coverage of the OH_{ads}. The above so-called bifunctional mechanism may be one of the reasons for the promoting effect of Au to Pd since the onset potential of the EOR on the Pd$_m$Au/C catalysts with relatively high m is much more negative with respect to that on the Pd/C catalyst. This suggested that the Au addition could facilitate the removal of the adsorbed intermediate species on the catalyst surface. In addition, the lattice

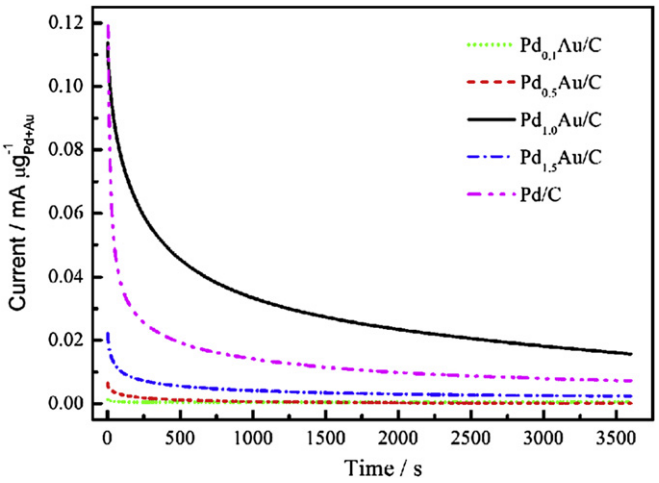

Fig. 7. Chronoamperograms of the Pd_mAu/C and Pd/C catalysts in 0.5 M KOH + 2.0 M CH_3COOH at −0.5 V.

strain, arising from the discrepancy between lattice parameters of the constitute metals, may be another reason for the enhanced catalytic activity of the bimetallic Pd–Au catalysts. Since the lattice parameter for Au (4.08 Å) is larger than that for Pd (3.89 Å), the lattice mismatch between Au and Pd could lead to an expansive strain of Pd and an up-shift of d-band center [40,41], which would weaken the interaction between the adsorbed intermediate species CH_3CO_{ads} and the surface of Pd and thus resulted in an enhanced activity toward EOR.

The long-term stability of Pd in the Pd_mAu/C and Pd/C catalysts was investigated by the chronoamperometry (CA) experiments (Fig. 7). All of the catalysts featured a pronounced current decay in the first 10 min due to the accumulation of poisonous intermediates, and then the current decay slowed down at longer times. The activity order of the Pd_mAu/C catalysts at the time of 60 min was similar to that obtained from the CV measurements. $Pd_{1.0}Au/C$ catalyst showed the highest current at the time of 60 min, exhibiting the highest stability for EOR. The highest MSA data was found at $m = 1.0$ (0.016 mA μg^{-1}_{Pd+Au}), which was *ca.* 2.2 times that of the Pd/C catalyst; the current decay was *ca.* 85% in 60 min, which was lower than that of the Pd/C catalyst (94%). These data suggested that the activity and stability of Pd could be significantly improved due to the co-presence of Au and $Pd_{1.0}Au/C$ exhibited the highest activity and stability for EOR among the Pd_mAu/C catalysts. Proper proximity of Au and Pd atoms on the surface of the NPs might be crucial to the catalytic performance. Recently, Sung et al. reported a similar result that the alloyed PtAu NPs containing equal Pt and Au atoms were highly active for HCOOH electro-oxidation [42], the MSA and IA of Pt was 3 and 5 times that of the alloyed PtAu NPs with the atomic Pt/Au ratio being 4:1, respectively. The third-body effect and the electronic modification of Pt might be the possible reasons for the enhanced activity. For the most active $Pd_{1.0}Au/C$ catalyst in this work, the proximity and relative amount of Au and Pd on the surface of the NPs, which resulted in a peculiar surface structure, might be responsible for the highly catalytic performance of Pd. However, more powerful measurements would be required to gain further insights into the details of such peculiar surface structure.

4. Conclusions

We demonstrated that the co-reduction of K_2PdCl_4 and $HAuCl_4$ precursors could lead to the formation of Pd_mAu alloy nanostructures. The addition of Au into Pd catalysts could significantly enhance the catalytic activity and stability of Pd for EOR in alkaline electrolyte in comparison with the monometallic Pd/C catalyst. The improvement was strongly dependent on the composition (atomic Pd/Au ratio) of the catalysts. PdAu NPs containing proper atomic Pd/Au ratio ($Pd_{1.0}Au$) showed the highest mass-specific activity, intrinsic activity and long-term stability toward EOR among the series of Pd_mAu/C catalysts. The proximity and relative amount of Au and Pd on the surface of the NPs would be responsible for the improvement of Pd in the alloyed Pd_mAu/C catalysts. These findings would have a promising application for designed preparation of bimetallic catalysts in direct alcohol fuel cells and other technologies.

Acknowledgments

This work is supported by Scientific Research Foundation for the Outstanding Young Scientist of Shandong Province (BS2011NJ009), Natural Science Foundation of Shandong Province (ZR2010EM026) and Initial Research Funding for the Doctors of Qufu Normal University (BSQD08036).

References

[1] C.K. Dyer, J. Power Sources 106 (2002) 31–34.
[2] S. Song, P. Tsiakaras, Appl. Catal. B 63 (2006) 187–193.
[3] V. Radmilovic, H.A. Gasteiger, P.N. Ross, J. Catal. 154 (1995) 98–106.
[4] T.S. Almeida, L.M. Palma, P.H. Leonello, C. Morais, K.B. Kokoh, A.R. De Andrade, J. Power Sources 215 (2012) 53–62.
[5] L.X. Ding, A.L. Wang, G.R. Li, Z.Q. Liu, W.X. Zhao, C.Y. Su, Y.X. Tong, J. Am. Chem. Soc. 134 (2012) 5730–5733.
[6] D.S. Su, G.Q. Sun, Angew. Chem. Int. Ed. 50 (2011) 11570–11572.
[7] Y. Wang, X. Wang, C.M. Li, Appl. Catal. B 99 (2010) 229–234.
[8] W.M. Wang, D. Zheng, C. Du, Z.Q. Zou, X.G. Zhang, B.J. Xia, H. Yang, D.L. Akins, J. Power Sources 167 (2007) 243–249.
[9] P.K. Shen, C.W. Xu, Electrochem. Commun. 8 (2006) 184–188.
[10] J.P. Liu, J.Q. Ye, C.W. Xu, S.P. Jiang, Y.X. Tong, Electrochem. Commun. 9 (2007) 2334–2339.
[11] C.W. Xu, H. Wang, P.K. Shen, S.P. Jiang, Adv. Mater. 19 (2007) 4256–4259.
[12] D. Kim, Y.W. Lee, S.B. Lee, S.W. Han, Angew. Chem. Int. Ed. 51 (2012) 159–163.
[13] T. Akita, T. Hiroki, S. Tanaka, T. Kojima, M. Kohyama, A. Iwase, F. Hori, Catal. Today 131 (2008) 90–97.
[14] F. Ksar, L. Ramos, B. Keita, L. Nadjo, P. Beaunier, H. Remita, Chem. Mater. 21 (2009) 3677–3683.
[15] S.Y. Shen, T.S. Zhao, J.B. Xu, Electrochim. Acta 55 (2010) 9179–9184.
[16] L.Q. Li, Y.F. E, J.M. Yuan, X.Y. Luo, Y. Yang, L.Z. Fan, Electrochim. Acta 56 (2011) 6237–6244.
[17] K.W. Park, J.H. Choi, B.K. Kwon, S.A. Lee, Y.E. Sung, H.Y. Ha, S.A. Hong, H. Kim, A. Wieckowski, J. Phys. Chem. B 106 (2002) 1869–1877.
[18] P. Strasser, S. Koh, T. Anniyev, J. Greeley, K. More, C. Yu, Z. Liu, S. Kaya, D. Nordlund, H. Ogasawara, M.F. Toney, A. Nilsson, Nat. Chem. 2 (2010) 454–460.
[19] V. Stamenkovic, B.S. Mun, K. Mayrhofer, P.N. Ross, N.M. Markovic, J. Rossmeisl, J. Greeley, J.K. Norskov, Angew. Chem. Int. Ed. 45 (2006) 2897–2901.
[20] M.H. Shao, P. Liu, J.L. Zhang, R. Adzic, J. Phys. Chem. B 111 (2007) 6772–6775.
[21] J.R. Kitchin, J.K. Norskov, M.A. Barteau, J.G. Chen, Phys. Rev. Lett. 93 (2004) 156801–156804.
[22] L. Zhang, J.W. Zhang, Q. Kuang, S.F. Xie, Z.Y. Jiang, Z.X. Xie, L.S. Zheng, J. Am. Chem. Soc. 133 (2011) 17114–17117.
[23] Y.W. Lee, N.H. Kim, K.Y. Lee, K. Kwon, M. Kim, S.W. Han, J. Phys. Chem. C 112 (2008) 6717–6722.
[24] M.H. Martin, A. Lasia, Electrochim. Acta 53 (2008) 6317–6322.
[25] A.E. Blozan, J. Electroanal. Chem. 380 (1995) 127–138.
[26] G. Denault, C. Milhano, D. Pletcher, Phys. Chem. Chem. Phys. 7 (2005) 3545–3551.
[27] J. Luo, P.N. Njoki, Y. Lin, L.Y. Wang, C.J. Zhong, Electrochem. Commun. 8 (2006) 581–587.
[28] Y.W. Lee, M. Kim, Y. Kim, S.W. Kang, J.H. Lee, S.W. Han, J. Phys. Chem. C 114 (2010) 7689–7693.
[29] W. Pan, X. Zhang, H.Y. Ma, J.T. Zhang, J. Phys. Chem. C 112 (2008) 2456–2461.
[30] L.Z. Mezey, J. Giber, Jpn. J. Appl. Phys. 21 (1982) 1569–1571.
[31] R. Anton, H. Eggers, J. Veletas, Thin Solid Films 226 (1993) 39–47.
[32] C.-W. Yi, K. Luo, T. Wei, D.W. Goodman, J. Phys. Chem. B 109 (2005) 18535–18540.
[33] J. Xu, T. White, P. Li, C.H. He, J.G. Yu, W.K. Yuan, Y.F. Han, J. Am. Chem. Soc. 132 (2010) 10398–10406.
[34] Y.Y. Feng, L.X. Bi, Z.H. Liu, D.S. Kong, Z.Y. Yu, J. Catal. 290 (2012) 18–25.

[35] Y. Lu, W. Chen, J. Phys. Chem. C 114 (2010) 21190–21200.
[36] Y. Liu, L.W. Wang, G. Wang, C. Deng, B. Wu, Y. Gao, J. Phys. Chem. C 114 (2010) 21417–21422.
[37] V. Mazumder, S.H. Sun, J. Am. Chem. Soc. 131 (2009) 4588–4589.
[38] Z.X. Liang, T.S. Zhao, J.B. Xu, L.D. Zhu, Electrochim. Acta 54 (2009) 2203–2208.
[39] F. Ksar, G. Surendran, L. Ramos, B. Keita, L. Nadjo, E. Prouzet, P. Beaunier, A. Hagège, F. Audonnet, H. Remita, Chem. Mater. 21 (2009) 1612–1617.
[40] J. Greeley, J.K. Norskov, M. Mavrikakis, Annu. Rev. Phys. Chem. 53 (2002) 319–348.
[41] Y. Wang, T.S. Nguyen, X.W. Liu, X. Wang, J. Power Sources 195 (2010) 2619–2622.
[42] I.S. Park, K.S. Lee, J.H. Choi, H.Y. Park, Y.E. Sung, J. Phys. Chem. C 111 (2007) 19126–19133.